The Transfinite-Element Time-Domain Method

Din-Kow Sun, *Member, IEEE*, Jin-Fa Lee, *Member, IEEE*, and Zoltan Cendes, *Member, IEEE*

***Abstract*—This paper presents an efficient time-domain method for computing the propagation of electromagnetic waves in microwave structures. The procedure uses high-order vector bases to achieve high-order accuracy in space, the Newmark's method to provide unconditional stability in time, and the transfinite-element method to truncate the waveguide ports. The resulting system matrix is real, symmetric, positive–definite, and can be solved by using the highly efficient multilevel preconditioned conjugate gradient algorithm. Since the method allows large time steps and nonuniform grids, the computational complexity for problems with irregular geometries is superior to the finite-difference time-domain method.**

***Index Terms*—Hierarchical vector bases, late-time instability, Newmark's scheme, scattering matrix, time-domain Maxwell's equations, transfinite-element method, vector finite-element method.**

I. Introduction

ALTHOUGH the finite-difference time-domain (FDTD) method is widely used to model electromagnetic-wave propagation in microwave structures, it has three major drawbacks. First, FDTD employs a low-order approximation in space that requires at least ten cells per wavelength to achieve acceptable accuracy. Second, FDTD's stability is tied to grid size through the Courant condition and imposes small time steps in structures involving fine details. Third, FDTD is not compliant with interface conditions in materials varying in both permittivity and permeability. Even newer conformal FDTD methods are not compliant because two grids are required [1]. These drawbacks necessitate the use of fine grids and many time steps and, thus, result in long solution times with large complex problems.

While FDTD has been very widely used in the past, finite-element time-domain (FETD) methods have also been developed in recent years [7]–[9]. FETD is an outgrowth of advances in finite-element frequency-domain (FEFD) methods [2]–[6]. In [7], an unconditionally stable FETD method is presented that circumvents the major drawbacks of FDTD. Advantages of FETD include the use of high-order vector basis functions to achieve high accuracy, unconditional stability to allow the time step to be taken independent of the mesh size, and the use of a single mesh that easily conforms to material interfaces. FETD provides more accurate solutions for a given mesh size, it allows the time step to depend on the rise/fall time of the input signal rather than the mesh size, and it adapts the mesh to fine details without requiring the mesh to be fine elsewhere.

This paper improves FETD in several ways. First, we rewrite the time-domain vector-wave equation in scaled time and space coordinates, making the new equation applicable to any dimensional scale. We then discretize the equation with the high-order hierarchical vector bases developed in [6]. These hierarchical basis functions bestow a hierarchical structure on the system matrix; this allows the system equation to be solved by using the efficient preconditioned conjugate gradient algorithm. Next, we employ the transfinite-element method [10] to couple the input and output waveguide ports to the three-dimensional (3-D) region. In the past, the absorbing boundary condition (ABC) [11] was applied at port boundaries. However, the ABC approach has limited success with multimode scattering because both the port impedance and mode patterns change with frequency. Thus, the ABC approach is limited to less dispersive cases such as microstrip problems with single-mode propagation. The transfinite-element method reduces the field unknowns on the ports to the coefficients of the modal expansion. It is proven in [12] that the transfinite-element method produces unitary scattering matrices. Thus, the method yields more accurate solutions than the ABC approach. Finally, Newmark's method is used to derive an unconditionally stable second-order finite-difference equation in time.

II. Formulation

A. Scaled Time-Domain Vector Wave Equation

Maxwell's equations yield the following time-domain vector-wave equation in source-free regions:

$$\nabla \times \frac{1}{\mu_r} \nabla \times \vec{E} + \frac{\varepsilon_r}{c^2} \frac{\partial^2 \vec{E}}{\partial t^2} + \mu_r \sigma \frac{\partial \vec{E}}{\partial t} = 0, \qquad \text{in } \Omega. \quad (1)$$

Here, $\vec{E}$ is the electric field and σ, ε_r, and μ_r are the conductivity, relative permittivity, and relative permeability, respectively. The boundary conditions to be imposed on (1) are

$$\begin{aligned} \vec{E} \times \hat{n} &= 0, \qquad \text{on } \Gamma_E \\ \nabla \times \vec{E} &= \frac{1}{c} \frac{\partial \vec{E}}{\partial t} \times \hat{n}, \qquad \text{on } \Gamma_\infty. \end{aligned} \quad (2)$$

Here, $\hat{n}$ denotes the outward unit normal of the surface. Let ω_0 be the highest angular frequency of interest. Scaling time as $t' = \omega_0 t$, (1) becomes

$$\nabla \times \frac{1}{\mu_r} \nabla \times \vec{E} + k_0^2 \varepsilon_r \frac{\partial^2 \vec{E}}{\partial t'^2} + \mu_0 \sigma \omega_0 \frac{\partial \vec{E}}{\partial t'} = 0 \quad (3)$$

Manuscript received February 27, 2003; revised April 30, 2003.

D.-K. Sun and Z. Cendes are with the Ansoft Corporation, Pittsburgh, PA 15219 USA.

J.-F. Lee is with the Department of Electrical Engineering, The Ohio State University, Akron, OH 43210 USA.

Digital Object Identifier 10.1109/TMTT.2003.817457

where $k_0 = \omega_0/c$ and μ_0 is the permeability of air. Further scaling the spatial coordinates as $x' = k_0 x$ and the differential operator as $\nabla' = \nabla/k_0$ yields

$$\nabla' \times \frac{1}{\mu_r}\nabla' \times \vec{E} + \varepsilon_r \frac{\partial^2 \vec{E}}{\partial t'^2} + \sigma' \frac{\partial \vec{E}}{\partial t'} = 0 \tag{4}$$

where $\sigma' = ((\mu_0 \sigma \omega_0)/k_0^2)$. Using the same transformations, the ABC (2) becomes

$$\nabla' \times \vec{E} = \frac{\partial \vec{E}}{\partial t'} \times \hat{n}, \qquad \text{on } \Gamma_\infty. \tag{5}$$

For the sake of simplicity, we will drop the prime signs and employ the new time and space coordinate scales everywhere in the following.

B. Discretization in Space

Applying the Galerkin's method and Green's theorem to (4) yields the following bilinear functional:

$$\begin{aligned} 0 = & F(\vec{E}_*, \vec{E}) \\ = & \int \nabla \times \vec{E}_* \cdot \frac{1}{\mu_r} \nabla \times \vec{E} dV + \int \vec{E}_* \cdot \varepsilon_r \frac{\partial^2}{\partial t^2} \vec{E} dV \\ & + \int \vec{E}_* \cdot \sigma \frac{\partial}{\partial t} \vec{E} dV + \int_{\Gamma_\infty} (\vec{E}_* \times \hat{n}) \cdot \frac{\partial}{\partial t} (\vec{E} \times \hat{n}) da \\ & + \mu_0 \mathrm{c} \int_{\Gamma_\mathrm{p}} \left(\vec{E}_* \times \frac{\partial}{\partial t} \vec{H} \right) \cdot \hat{n} da \end{aligned} \tag{6}$$

where Γ_p is the port boundary. Now we write the testing and trial vectors as a linear combination of the vector basis set $\{\vec{\alpha}_i\}$

$$\vec{E}_* = \sum_i \vec{\alpha}_i (e_*)_i \quad \vec{E} = \sum_i \vec{\alpha}_i (e)_i.$$

Here, $(e_*)_i$ and $(e)_i$ are the coefficients multiplying the basis functions. Equation (6) becomes

$$\begin{aligned} (e_{*I}^t \; e_{*P}^t) & \left\{ \begin{bmatrix} M_{II} & M_{IP} \\ M_{PI} & M_{PP} \end{bmatrix} \frac{\partial^2}{\partial t^2} \begin{pmatrix} e_I \\ e_P \end{pmatrix} + \begin{bmatrix} K_{II} & K_{IP} \\ K_{PI} & K_{PP} \end{bmatrix} \begin{pmatrix} e_I \\ e_P \end{pmatrix} \right\} \\ & + \begin{bmatrix} B_{II} & B_{IP} \\ B_{PI} & B_{PP} \end{bmatrix} \frac{\partial}{\partial t} \begin{pmatrix} e_I \\ e_P \end{pmatrix} \Bigg\} \\ & = -\mu_0 \mathrm{c} \int_{\Gamma_\mathrm{p}} \left(\vec{E}_* \times \frac{\partial}{\partial t} \vec{H} \right) \cdot \hat{n} da \end{aligned} \tag{7}$$

where the subscripts I and P signify the interior and port unknowns and

$$\begin{aligned} K_{ij} &= \int \frac{1}{\mu_r} \nabla \times \vec{\alpha}_i \cdot \nabla \times \vec{\alpha}_j d\Omega \\ M_{ij} &= \int \varepsilon_r \vec{\alpha}_i \cdot \vec{\alpha}_j d\Omega \\ B_{ij} &= \int \sigma \vec{\alpha}_i \cdot \vec{\alpha}_j d\Omega + \int_{\Gamma_\infty} (\vec{\alpha}_i \times \hat{n}) \cdot (\vec{\alpha}_j \times \hat{n}) d\Gamma. \end{aligned}$$

As discussed in [6], to optimize the performance of the matrix solver, we need to maximize the mutual orthogonality among the basis vectors themselves and among their curls.

C. Transfinite-Element Method

At waveguide ports, we write the transverse components of the testing and trial solutions on the port boundary Γ_p as a superposition of modal solutions

$$\begin{aligned} \vec{\mathrm{E}}_{*_\mathrm{p}} &= \sum_{i=1}^{m} a_{*_{pi}}(t) \vec{E}_{pi}(\omega_0) \\ \vec{\mathrm{E}}_\mathrm{p} &= \delta_{p1} \mathrm{I(t)} \vec{E}_{11}(\omega_0) + \sum_{i=1}^{m} a_{pi}(t) \vec{E}_{pi}(\omega_0). \end{aligned} \tag{8}$$

Here, $\mathrm{I(t)}$ is the amplitude function of the input signal, the a_{pi}'s are the unknown modal coefficients of the ith mode at the pth port, and the $\vec{E}_{pi}(\omega_0)$'s are the corresponding eigenmodes of the transverse electric field at the frequency ω_0. Equation (8) is an accurate approximation provided the field patterns stay similar as the frequency varies. This is true in the case of homogeneous waveguides and microstrip lines. In the same way, the transverse magnetic field can be written in the terms of the eigenmodes of the transverse magnetic fields as follows:

$$\vec{\mathrm{H}}_\mathrm{p} = -\delta_{p1} \mathrm{I(t)} \vec{H}_{11}(\omega_0) + \sum_{i=1}^{m} a_{pi}(t) \vec{H}_{pi}(\omega_0).$$

Here, the minus sign in front of the input field indicates that the input wave travels in the opposite direction.

By orthogonality of waveguide modes, we know that

$$\int_{\Gamma_p} \left(\vec{E}_{pi}(\omega_0) \times \vec{H}_{pj}(\omega_0) \right) \cdot \hat{n} da = \delta_{ij}.$$

The right-hand side of (7) can be integrated to give $-\mu_0 c a_*^t (\partial/\partial t)(-\mathrm{I(t)} i + a)$, where the column vector i contains 1 at the first entry and 0 elsewhere. Further, setting the interior values equal to the port values along port boundaries imposes continuity of the field vectors. Hence, from (8), e_P and e_{*P} are written in terms of a port-mapping matrix P as

$$e_P = P\,(\mathrm{I(t)} i + a) \equiv P a' \quad e_{*P}^t = a_*^t P^t.$$

Plugging the above equations into (7) gives the transfinite-element matrix equation

$$M \frac{\partial^2 e}{\partial t^2} + B \frac{\partial e}{\partial t} + K e = b \tag{9}$$

where

$$\begin{aligned} M &= \begin{bmatrix} M_{II} & M_{IP} P \\ P^t T_{PI} & P^t M_{PP} P \end{bmatrix} \\ K &= \begin{bmatrix} K_{II} & K_{IP} P \\ P^t K_{PI} & P^t K_{PP} P \end{bmatrix} \\ B &= \begin{bmatrix} B_{II} & B_{IP} P \\ P^t B_{PI} & P^t B_{PP} P + \mu_0 c \end{bmatrix} \\ e &= \begin{pmatrix} e_I \\ a' \end{pmatrix} \\ b &= 2\mu_0 c \frac{\partial}{\partial t} \mathrm{I}(t) \begin{pmatrix} 0 \\ i \end{pmatrix}. \end{aligned}$$

The transfinite-element method reduces the number of unknowns, but makes the system matrices denser by adding m

full columns, where m is the number of modal coefficients. If there are N^2 unknowns on a port, the number of added entries is mN^2. In the ABC approach, the part of the system matrix linked to the port has aN^2 nonzero entries, where a is the number of nonzero entries per row. In most cases, the computational cost of both methods is comparable.

D. Discretization in Time

Newmark's method provides the following second-order difference equation in time:

$$M\frac{e^{n+1}-2e^n+e^{n-1}}{\Delta t^2}+B\frac{e^{n+1}-e^{n-1}}{2\Delta t}+K\frac{e^{n+1}+2e^n+e^{n-1}}{4}=b^n. \quad (10)$$

Given two starting vectors e^{-1} and e^0, e^n is computed through the iteration

$$d^{n+1}=d^n+A^{-1}\left(b^n\Delta t^2-B\Delta t d^n-Ke^n\Delta t^2\right) \quad (11)$$

where

$$d^n=e^n-e^{n-1}$$
$$A=M+\frac{B\Delta t}{2}+\frac{K\Delta t^2}{4}.$$

Finally, the scattering matrix S is obtained by dividing the Fourier components of the modal coefficients of the output signal by the corresponding components of the input signal.

III. Performance Issues

A. Performance Comparison With the Frequency-Domain Formulation

Both the time- and frequency-domain methods have certain advantages and disadvantages. Some problems, e.g., nonlinear materials, can only be solved in the time domain, while some problems, e.g., dispersive materials, are more easily solved in the frequency domain. The types of the solutions are also different: time-domain methods provide transient solutions, while frequency-domain methods provide time–harmonic solutions. The best approach to use depends on the needs of the particular problem being solved. The following advantages and disadvantages of the time-domain formulation are observed.

Advantages

1) The time-domain system matrix A is pure real, while the frequency-domain transfinite-element method system matrix generates a few complex entries.
2) The time-domain system matrix is positive–definite, while the system matrix in the frequency-domain formulation is indefinite. For this reason, the time-domain matrix converges much faster using an iterative preconditioned conjugate gradient solver.
3) Broad-band solution is a natural outcome of the time-domain simulation; in the frequency domain, one must employ a model order-reduction algorithm [12].
4) The zero-frequency instability of the frequency-domain formulation [13] does not occur in the time-domain formulation. This is because the M matrix dominates the system matrix in the time-domain formulation, while the K matrix dominates in the frequency-domain formulation. Zero frequency in the frequency domain corresponds to an infinite time step in the time domain, which does not happen in practical numerical simulations. At the other extreme of approaching a zero time step, the time-domain formulation does not produce a singular matrix either. In fact, the technique used to overcome the frequency-domain zero-frequency instability, the tree–cotree splitting of the edge bases, worsens the condition number of the system matrix and, for that reason, the splitting is counterproductive and not recommended. This has been confirmed by numerical experiments.

Disadvantages

1) As discussed later, there is a mild late-time instability if the simulation is carried on long enough.
2) In the case of high-Q or filter circuits, the time-domain formulation requires long simulation times because the inner structure traps the incident wave, releasing energy slowly back to the ports.
3) Due to truncation errors in time, the time-domain solution is less accurate than the frequency-domain solution.

Problems associated with late-time instability and long simulation times can be avoided by using the matrix pencil method [14]. The matrix pencil method computes the poles and residues of the system and uses them to predict the late-time response. In this way, the simulation is completed before late-time instability sets in.

B. Termination Criterion

The question of "when to terminate" arises in many numerical simulations. Without a termination criterion, one cannot judge whether the new method is more efficient than the existing one. Here, we terminate the simulation according to the following procedure.

- We first determine the instant that the input pulse reaches the output ports by monitoring the scattering coefficients.
- We continue the simulation for a period of time that is twice the pulsewidth of the input signal, but terminate early if the total energy exiting to the ports is close to the input energy.

C. Late-Time Instability

If the excitation is periodic, the steady-state solution of (10) is also periodic. By plugging $e^{n+1}=\exp(j\Delta t)e^n$ and $e^{n-1}=\exp(-j\Delta t)e^n$ into (10), one can prove that e^n satisfies the matrix equation resulting from the frequency-domain formulation up to second order in time. This shows that with a periodic excitation, time marching arrives at the same solution as the frequency-domain formulation. Unfortunately, (10) also carries a dc solution. For the sake of discussion, let us assume the microwave structure is filled with air and shielded by a perfect

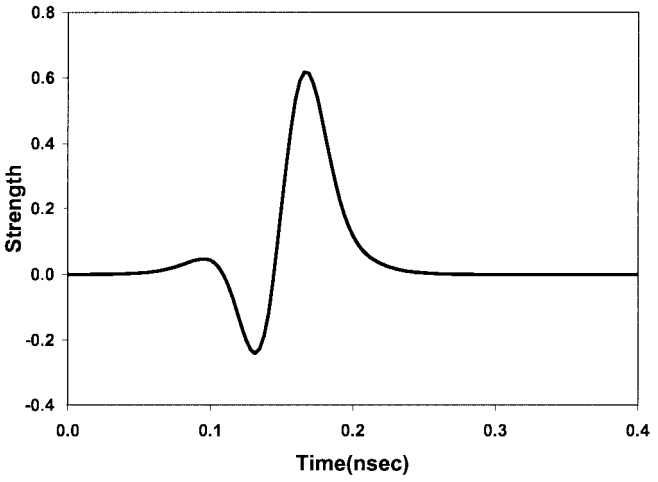

(a)

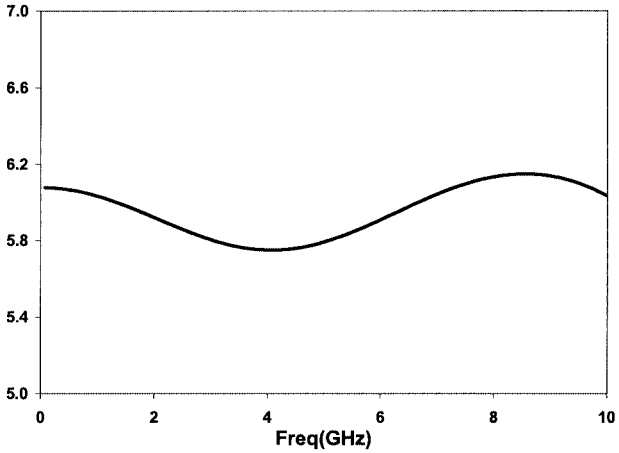

(b)

Fig. 1. Mixed-Gaussian pulse. (a) Time series. (b) Spectral content.

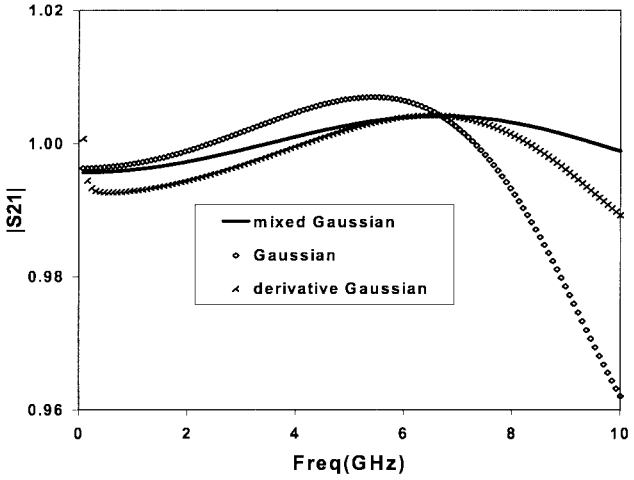

(a)

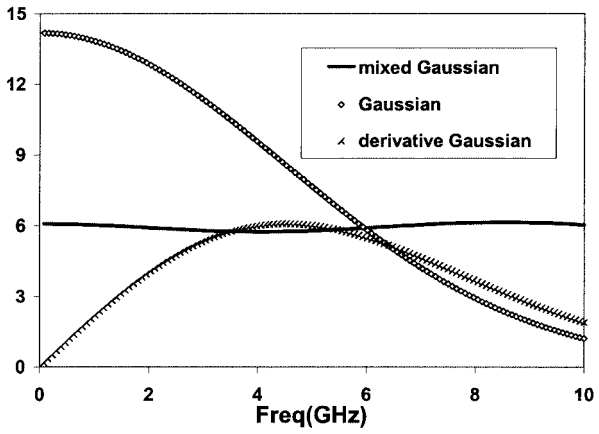

(b)

Fig. 2. Effect of the spectral content of the input signal for the coaxial waveguide. (a) Transmitted scattering amplitudes. (b) Spectral content of the input signals.

conductor. It is observed that (9) allows the following nontrivial dc solution [15]:

$$e_{\rm dc} = \big(e_{\rm rot} = 0, e_{\rm grad}, a' = 0\big)t.$$

Here, $e_{\rm rot}$ and $e_{\rm grad}$ are the coefficients of the rotational and gradient components of the field vector. Thus, the numerical contamination induced by the dc solution grows linearly in time, but is not as severe as the instability resulting from violating the Courant condition in the FDTD algorithm where the spurious solutions grow exponentially in time. More significantly, the scattering coefficients are unaffected by the dc solution. This provides another intrinsic advantage of the transfinite-element method.

D. Renormalization of Port Impedance

When dealing with nonmicrostrip ports, the impedances of the ports vary significantly with frequency. In deriving the system equation, we assumed that the port is terminated with the impedance corresponding to the highest frequency of interest. We, therefore, need to renormalize the computed scattering matrix to the matching impedance. One can incorporate port dispersion into (8), and implement an expensive convolution integral to compute the frequency-dependent terms. Here, we propose a simpler alternative requiring only a post-solution step. We first solve (11), and then transform the computed scattering matrix to the matched scattering matrix S_m according to the following two equations [16]:

$$Z = Z_{\omega_0}^{\frac{1}{2}}(1+S)(1-S)^{-1}Z_{\omega_0}^{\frac{1}{2}}$$
$$S_m = \left(Z_\omega^{-\frac{1}{2}} Z Z_\omega^{-\frac{1}{2}} - 1\right)\left(Z_\omega^{-\frac{1}{2}} Z Z_\omega^{-\frac{1}{2}} + 1\right)^{-1}.$$

Z_ω is a diagonal matrix with diagonal entries defined by the port impedance at the angular frequency ω. Since the waveguide impedance contains poles, rational polynomials are used to fit the impedance curve.

E. Excitation Signal

To achieve uniform accuracy across the frequency band of interest, the spectral content of the input signal should be perfectly flat. However, an input signal of short duration is desirable so that time marching can be terminated as soon as the input signal passes through the system. Traditionally, time-domain methods have employed a Gaussian pulse or a derivative-Gaussian pulse for input. Unfortunately, both spectrums vary significantly within the band of interest. While

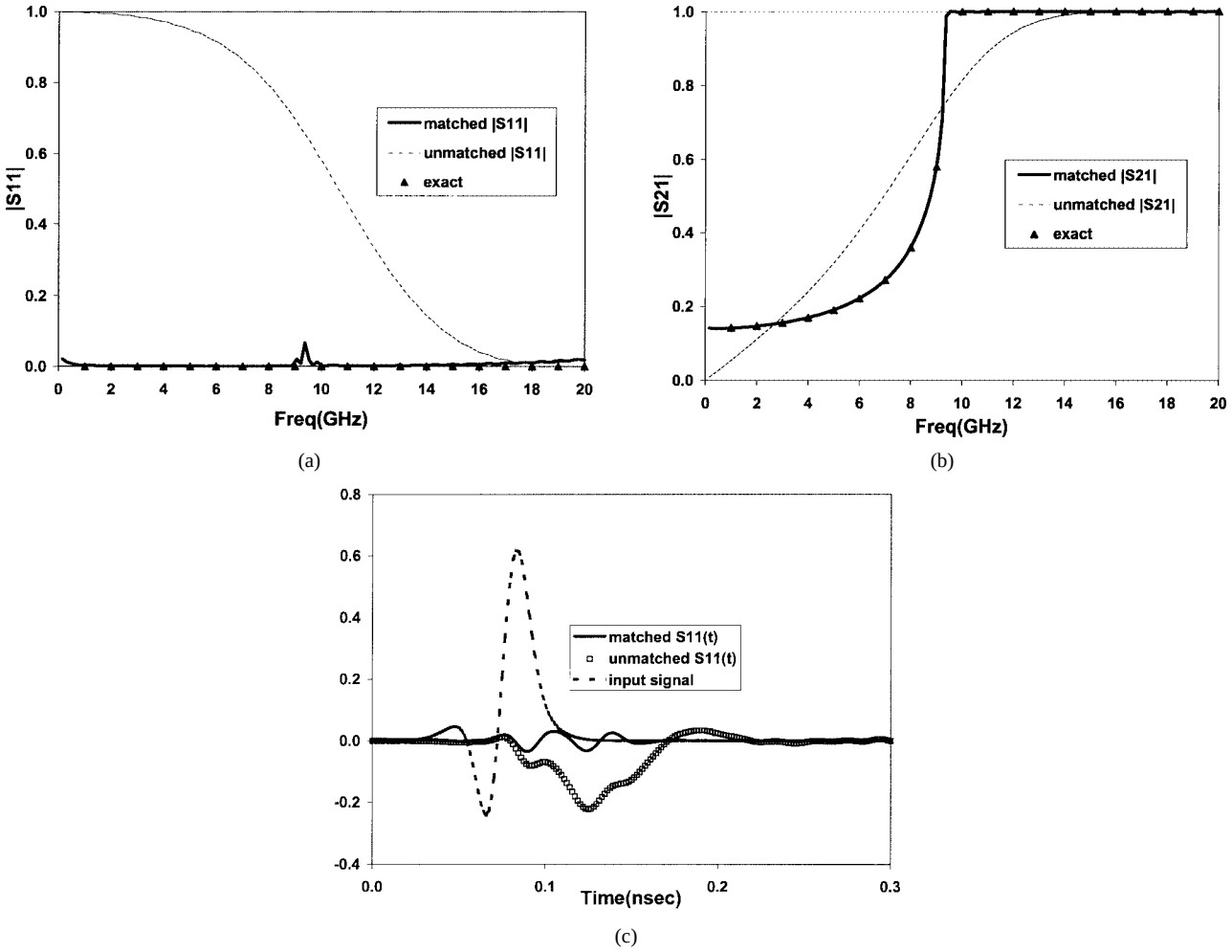

Fig. 3. Comparison of unmatched and matched scattering amplitudes for the rectangular waveguide. (a) $S11(f)$. (b) $S21(f)$. (c) $S11(t)$.

the Gaussian pulse peaks at dc and has low spectral content at the high end, the derivative-Gaussian pulse does not have a dc component. To compensate for the low spectral content at the trailing end of the Gaussian pulse, we add a derivative-Gaussian pulse designed to peak at the highest frequency of interest

$$\mathrm{I}(\tau) = 0.214 \exp\left(-\tau^2\right) + 2\tau \exp\left(-4\tau^2\right)$$

where $\tau = 2f_0(t - 1.5/f_0)$, and f_0 is the highest frequency of interest. Fig. 1 shows the input signal in both the time and frequency domains for $f_0 = 10$ GHz. We observe that the spectral content of the mixed-Gaussian pulse is relatively flat.

IV. Numerical Results

We now demonstrate the procedure with the following five examples:

1) coaxial waveguide;
2) rectangular waveguide;
3) microstrip low-pass filter;
4) asymmetrical waveguide step;
5) shielded rectangular dielectric waveguide.

The ports are solved using the full-wave procedure of [18]. To obtain an appropriate 3-D mesh, the problems are first solved in the frequency domain and the mesh is adaptively refined at the highest frequency of interest [17]. The meshes are then used to run time-domain simulations with the mixed-Gaussian pulse applied at the ports. A manually seeded mesh containing eight points per wavelength and refined around singular corners and edges can yield an accurate solution as well. If high-order bases are used, the number of points per wavelength can be reduced accordingly. In the following, the solutions of the proposed method are validated by either analytical or FEFD solutions.

A. Coaxial Waveguide

To demonstrate the effects of the spectral content of the input signal, we solve for the scattering matrix of an empty coaxial waveguide with an inner diameter of 0.07 in, an outer diameter of 0.232 in, and 1-in long, equivalent to 0.85λ at 10 GHz. Since the propagating mode is the nondispersive TEM mode, the problem of waveguide dispersion does not exist. The simulation was terminated at the 112th time step when the energy conservation error reached 1e-4. At each time step, the multilevel preconditioned gradient method took five iterations to reduce the relative residual to 1e-4. Since the mesh in this problem is uniform, an explicit scheme such as the FDTD method would have performed more rapidly in this case. However, as the following example shows, a much smaller mesh can be used with high-order bases, making the proposed method a competitive alternative. Fig. 2(a) shows the computed transmitted scattering

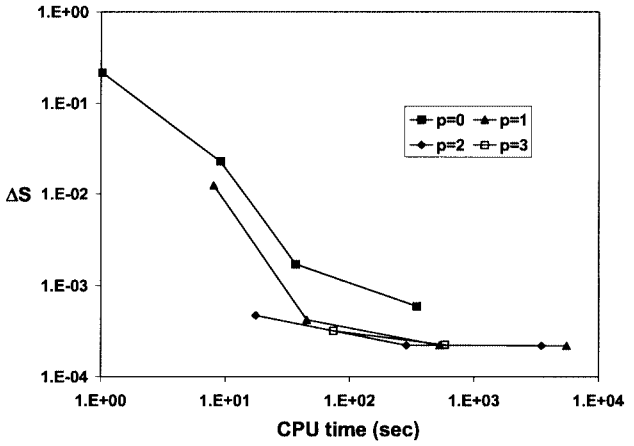

Fig. 4. Comparison of rates of convergence for the rectangular waveguide.

amplitudes for three types of the input signals. The spectral content of these three signals are plotted in Fig. 2(b). The scattering amplitudes exhibit relatively larger errors at frequencies with lower input amplitudes.

B. Empty Rectangular Waveguide

Since the port impedances are not matched in the proposed method, here we examine the effect of this approach. We study a rectangular waveguide of dimensions of 8×16 mm^2 and 10-mm long. Fig. 3(a) and (b) compares the scattering amplitudes before and after renormalization with the exact solution. Above cutoff, the unmatched scattering amplitudes show signs of dispersion; below cutoff, the waveguide is completely mismatched to the assumed impedance at the ports and the wave is totally reflected. Indeed, the port impedance below cutoff is pure imaginary, indicating a lossy port. If the port impedance were matched, the wave would travel through the ports and this would take only 0.35 ns, equal to the pulsewidth plus the time needed to travel from the input to output port. Since evanescent modes are bounced between the ports, it takes 0.8 ns for the wave to die out inside the structures. Fig. 3(c) shows that the matched reflected wave has a smaller amplitude than the unmatched one, revealing the consequence of the unmatched port impedance.

To demonstrate the benefit of using high-order bases in space, we solve a series of uniformly refined meshes with the order of the range space of the bases rising from zero to three. The average error versus CPU time is plotted in Fig. 4 where the error is computed as

$$\Delta S = \frac{\int_{f_1}^{f_2} \left(\left| |S_{21}|^2 - |S_{21}^{ex}|^2 \right| \right) df}{(f_2 - f_1)}.$$

Error in the time-domain simulation has two parts: discretization error in space and truncation error in time. In Fig. 4, we see that the higher order bases are more accurate with small meshes, but reach a plateau of 2.2e-4 when time truncation error dominates. To further lessen total error, one must reduce the time step, which is confirmed by numerical experiment. We observe in Fig. 5(a) and (b) that the errors at the cutoff frequency are often larger and converge slower than those at the other frequency points. The cutoff frequency point behaves like a singular point in the time coordinate, analogous to corners in space coordinates.

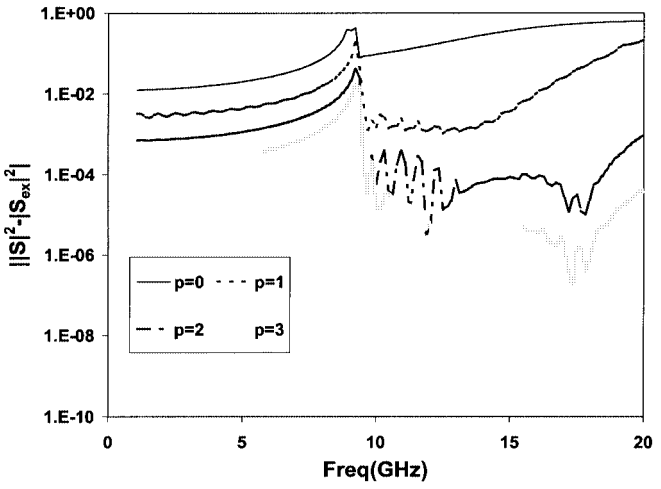

(a)

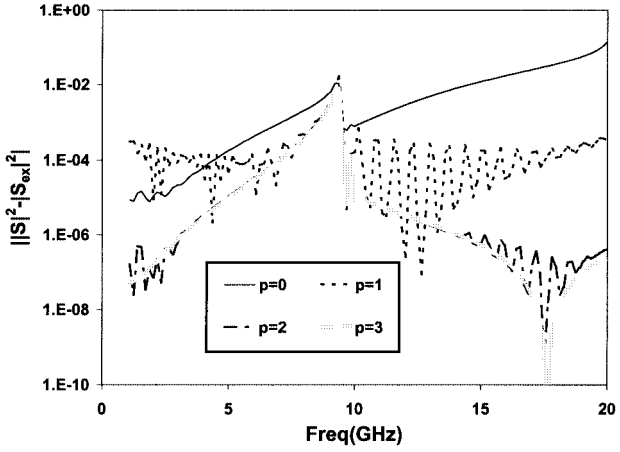

(b)

Fig. 5. Distribution of error for the rectangular waveguide. (a) Element size $= h$. (b) Element size $= h/2$.

C. Microstrip Low-Pass Filter

To show that the proposed method can be applied to microstrip structures, we consider a microstrip low-pass filter. The top view of the filter is depicted in Fig. 6. The substrate is 25-mil thick, and has a relative dielectric constant of 9.6. Due to the presence of three stubs, the spectral response of this filter from 2 to 20 GHz contains three poles. The time-domain solution is compared to a discrete sampling of the frequency-domain solution in Fig. 7. Due to singularities around the edges of the conducting strip, the mesh is extremely fine in these regions. If an explicit scheme has been used, the time step would need to be orders of magnitude smaller than is required here.

D. Asymmetrical Waveguide Step

To demonstrate the multimode capability of the transfinite-element method, we solve an asymmetrical rectangular waveguide step where one propagating mode from the input port is split into two modes at the output port. The dimensions of the

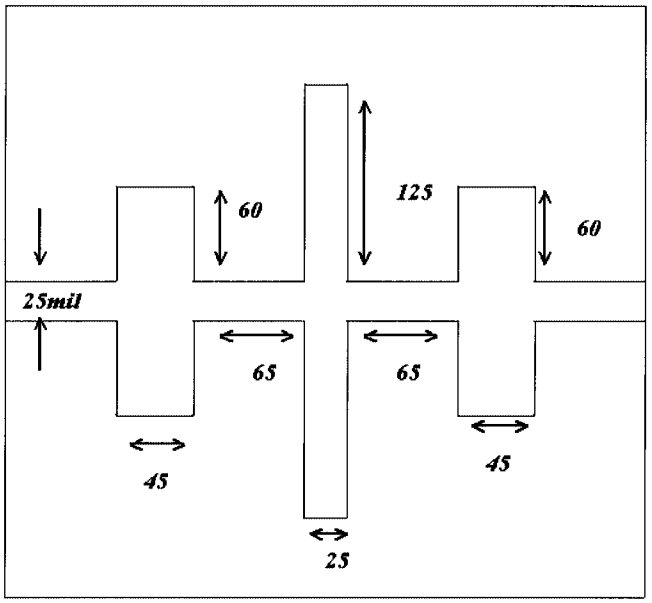

Fig. 6. Top view of a microstrip low-pass filter.

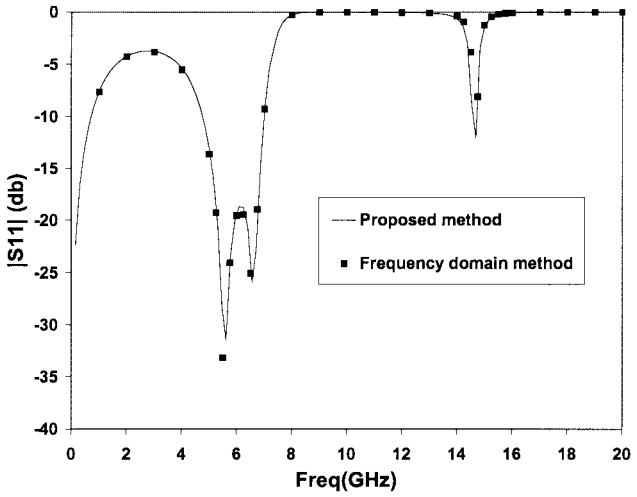

Fig. 7. Reflected scattering amplitude of the low-pass filter.

waveguide are changed from $2 \times 6\,\mathrm{mm}^2$ to $3 \times 9\,\mathrm{mm}^2$, as shown in Fig. 8(a). The cutoff frequency of the TE01 mode of the narrower guide is 25 GHz and the cutoff frequencies of the TE01 and TE02 modes of the wider guide are 17 and 33 GHz, respectively. To obtain the scattering matrix up to 35 GHz, we need to allow two modes for the wider guide and one mode for the narrower guide. The results are in excellent agreement with the frequency-domain solution, as shown in Fig. 8(b) where $S(i\_j, k\_l)$ is the entry of the generalized scattering matrix from port i, mode j to port k, mode l. Fig. 9 illustrates how the input signal from the narrower guide is split into two modes at the port of the wider guide.

E. Shielded Rectangular Dielectric Waveguide

To extend the applicability of the proposed method to the structures with port extensions other than homogeneous waveguides or microstrip lines, we consider the shielded rectangular dielectric waveguide shown in the insert of the Fig. 10. In this

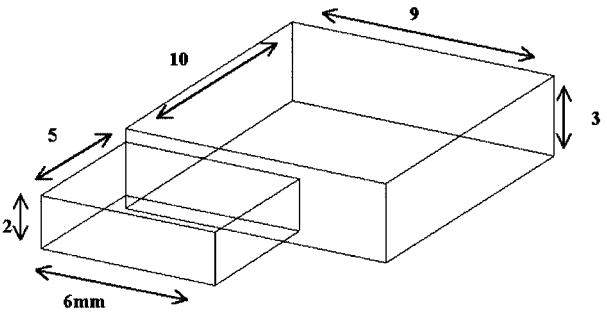

(a)

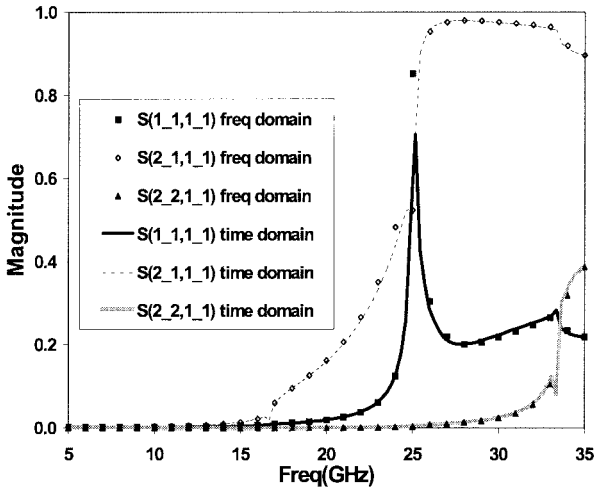

(b)

Fig. 8. (a) Asymmetrical waveguide step. (b) Transmitted scattering amplitudes of the asymmetrical waveguide step.

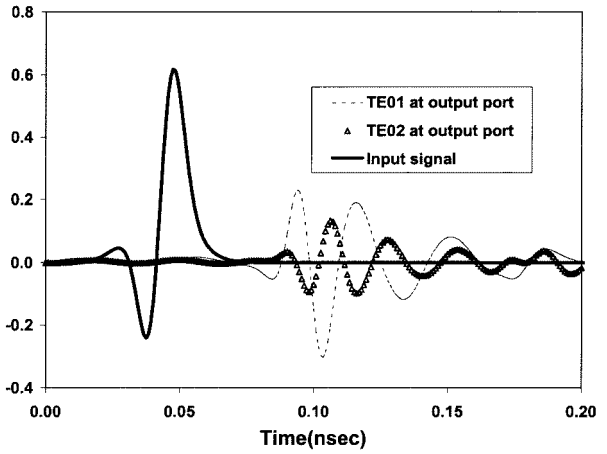

Fig. 9. Comparison of input and output time series for the asymmetrical waveguide step.

waveguide, the modes are hybrid, neither TE, nor TM. We compare the transmitted scattering amplitudes from the proposed method with those of the frequency-domain method. As shown in Fig. 11, large errors appear for the second mode at the low-frequency end. To inspect the cause, we plot the similarity index of the mode pattern versus frequency in Fig. 12. The similarity index of the mode pattern is defined as

$$\mathrm{SMP}(f) = 100 \times \left(1 - \left|\frac{(\vec{e}_f - \vec{e}_{f_0})^2}{\vec{e}_{f_0}^2}\right|\right)$$

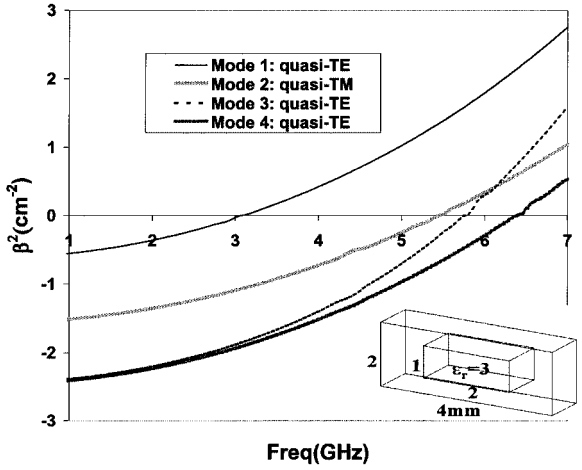

Fig. 10. Propagation constants of the shielded rectangular dielectric waveguide.

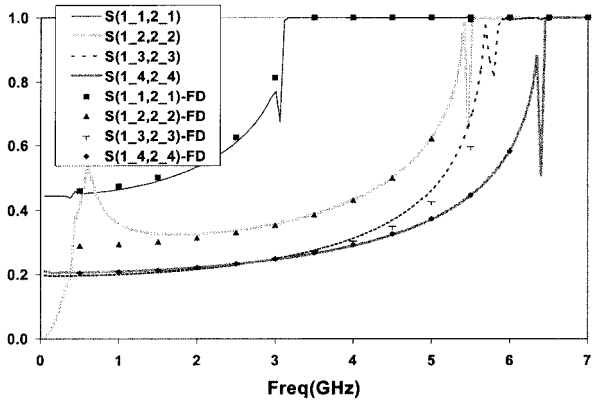

Fig. 11. Transmitted scattering amplitudes of the shielded rectangular dielectric waveguide.

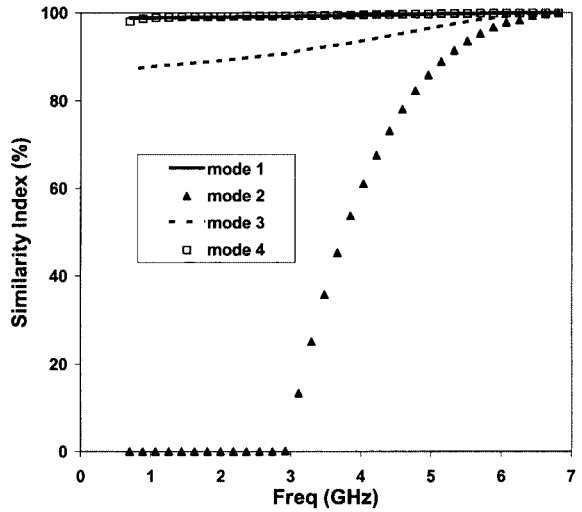

Fig. 12. Similarity index of the mode pattern for the shielded rectangular dielectric waveguide.

where $\vec{e}_f$ is the port solution at the frequency f. We discover the mode pattern of the second mode below 3 GHz does not resemble the mode pattern at 7 GHz. Therefore, in this case, the proposed method cannot be applied to the second mode. This example demonstrates our earlier contention that for structures with other than homogeneous waveguide or microstrip ports, one needs to compute the similarity index up front to determine the applicability of the proposed method.

V. Conclusions

A highly efficient procedure has been presented for the time solution of 3-D microwave structures. The proposed method has three major advantages over the FDTD method. First, the procedure requires a much smaller mesh than FDTD. This is achieved by employing unstructured meshes, high-order bases, and the transfinite-element method. Second, the procedure employs an unconditionally stable time-marching process that allows larger time steps. Third, the procedure uses only one conforming mesh and, hence, permits exact modeling of interfaces between materials with both permittivity and permeability variations. Numerical examples demonstrate the efficacy and applicability of the proposed method.

References

[1] W. Yu and R. Mittra, "A conformal finite difference time domain technique for modeling curved dielectric surfaces," *IEEE Microwave Wireless Comp. Lett.*, vol. 1, pp. 25–27, Jan. 2001.

[2] Z. Cendes, "Vector finite elements for electromagnetic field computation," *IEEE Trans. Magn.*, vol. 27, pp. 3958–3966, Sept. 1991.

[3] J. S. Savage and A. F. Peterson, "Higher-order vector finite elements for tetrahedral cells," *IEEE Trans. Microwave Theory Tech.*, vol. 44, pp. 874–879, June 1996.

[4] L. S. Andersen and J. L. Volakis, "Hierarchical tangential vector finite elements for tetrahedral," *IEEE Microwave Guided Wave Lett.*, vol. 8, pp. 127–129, Mar. 1998.

[5] J. P. Webb, "Hierarchal vector basis functions of arbitrary order for triangular and tetrahedral finite elements," *IEEE Trans. Antennas Propagat.*, vol. 47, pp. 1244–1253, Aug. 1999.

[6] D.-K. Sun, J.-F. Lee, and Z. Cendes, "Construction of nearly orthogonal Nedelec bases for rapid convergence with multilevel preconditioned solvers," *Siam J. Sci. Comput.*, vol. 23, no. 4, pp. 1053–1076, Oct. 2001.

[7] J.-F. Lee, R. Lee, and A. Cangellaris, "Time-domain finite-element methods," *IEEE Trans. Antennas Propagat.*, vol. 45, pp. 430–442, Mar. 1997.

[8] K. S. Komisarek, N. N. Wang, A. K. Dominek, and R. Hann, "An investigation of new FETD/ABC methods of computation of scattering from three-dimensional material objects," *IEEE Trans. Antennas Propagat.*, vol. 47, pp. 1579–1585, Oct. 1999.

[9] H.-P. Tsai, Y. Wang, and T. Itoh, "An unconditionally stable extended (USE) finite-element time-domain solution of active nonlinear microwave circuits using perfectly matched layers," *IEEE Trans. Microwave Theory Tech.*, vol. 50, pp. 2226–2232, Oct. 2002.

[10] Z. Cendes and J.-F. Lee, "The transfinite element method for modeling MMIC devices," *IEEE Trans. Microwave Theory Tech.*, vol. 36, pp. 1639–1649, Dec. 1988.

[11] A. Federico, P. Mezzanotte, L. Roselli, and R. Sorrentino, "A revised formulation of modal absorbing and matched modal source boundary conditions for the efficient FDTD analysis of waveguide structures," *IEEE Trans. Microwave Theory Tech.*, vol. 48, pp. 50–59, Jan. 2000.

[12] D.-K. Sun, Z. Cendes, and J.-F. Lee, "ALPS—A new fast frequency-sweep procedure for microwave devices," *IEEE Trans. Microwave Theory Tech.*, vol. 49, pp. 398–402, Feb. 2001.

[13] J. P. Webb and B. Forghani, "The low-frequency performance of H-ϕ and T-Ω methods using edge elements for 3D Eddy current problem," *IEEE Trans. Magn.*, vol. 29, pp. 2461–2463, Nov. 1993.

[14] T. K. Sarkar and O. Pereira, "Using the matrix pencil method to estimate the parameters of a sum of complex exponentials," *IEEE Antennas Propagat. Mag.*, vol. 37, pp. 48–55, Feb. 1995.

[15] C.-T. Hwang and R.-B. Wu, "Treating late-time instability of hybrid finite-element/finite-difference time-domain method," *IEEE Trans. Antennas Propagat.*, vol. 47, pp. 227–232, Feb. 1999.

[16] K. C. Gupta, R. Garg, and R. Chadha, *Computer-Aided Design of Microwave Circuits*. Norwood, MA: Artech House, 1981.

[17] D.-K. Sun, Z. Cendes, and J.-F. Lee, "Adaptive mesh refinement, H-version, for solving multiport microwave devices in three dimensions," *IEEE Trans. Magn.*, vol. 36, pp. 1596–1599, July 2000.

[18] J.-F. Lee, D.-K. Sun, and Z. Cendes, "Full-wave analysis of dielectric waveguides using tangential vector finite elements," *IEEE Trans. Microwave Theory Tech.*, vol. 39, pp. 1262–1271, Aug. 1991.

Din-Kow Sun (M'89) was born in Taipei, Taiwan, R.O.C., in 1956. He received the B.S. degree from the National Taiwan University, Taiwan, R.O.C., in 1978, and the Ph.D. degree from Carnegie–Mellon University, Pittsburgh, PA, in 1984, both in physics.

From 1984 to 1986, he was a Research Associate with the Department of Electrical and Computer Engineering, Carnegie–Mellon University. Since 1986, he has been a Research Engineer with the Ansoft Corporation, Pittsburgh, PA. His current research projects include the construction of vector singular bases and applications of domain decomposition and nonconforming finite-element methods (FEMs).

Jin-Fa Lee (S'85–M'85) received the B.S. degree from the National Taiwan University, Taiwan, R.O.C., in 1982, and the M.S. and Ph.D. degrees from Carnegie–Mellon University, Pittsburgh, PA, in 1986 and 1989, respectively, all in electrical engineering.

From 1988 to 1990, he was with the Ansoft Corporation, where he developed several computer-aided design (CAD)/computer-aided engineering (CAE) finite-element programs for modeling 3-D microwave and millimeter-wave circuits. His doctoral studies resulted in the first commercial 3-D FEM package (*HFSS*) for modeling RF/microwave components. From 1990 to 1991, he was a Post-Doctoral Fellow with the University of Illinois at Urbana-Champaign. From 1991 to 2000, he was with the Department of Electrical and Computer Engineering, Worcester Polytechnic Institute. He is currently an Associate Professor with the ElectroScience Laboratory, Department of Electrical Engineering, The Ohio State University, Akron. His current research interests are analyses of numerical methods, fast FEMs, integral-equation methods, hybrid methods, 3-D mesh generation, domain decomposition methods, and mortar finite elements.

Zoltan Cendes (S'67–M'73) received the B.S. degree in science engineering from The University of Michigan at Ann Arbor, in 1968, and the M.S. and Ph.D. degrees in electrical engineering from McGill University, Montreal, QC, Canada, in 1970 and 1972, respectively.

Upon graduation, he joined the General Electric Corporation, initially in the Large Steam-Turbine Generator Department and then in the Corporate Research and Development Center. During a portion of this time, he was also an Adjunct Associate Professor with Union College, Schenectady, NY. In 1980, he became an Associate Professor of electrical engineering with McGill University. In 1982, he joined the Faculty of Electrical and Computer Engineering with Carnegie–Mellon University, Pittsburgh, PA, where served as Professor until 1996 and, since then, as Adjunct Professor. He is also founder and Chairman of the Ansoft Corporation, Pittsburgh, PA, where he currently serves as the Chief Technology Officer responsible for directing the company's product and technology research. He has authored or coauthored over 200 journal and conference papers. He is on the Editorial Board of the *International Journal of RF and Microwave Computer-Aided Engineering*,

Dr. Cendes is a member of the IEEE Microwave Theory and Techniques Society (IEEE MTT-S) Technical Committee on CAD. He has served on the International Steering Committee of the COMPUMAG Conference and is a past chairman of the IEEE Conference on Electromagnetic Field Computation.